Observation of quantized subband states and evidence for surface electron accumulation in CdO from angle-resolved photoemission spectroscopy

L. F. J. Piper,[1] Leyla Colakerol,[1] P. D. C. King,[2] A. Schleife,[3] J. Zúñiga-Pérez,[4,*] Per-Anders Glans,[1] Tim Learmonth,[1] A. Federov,[5] T. D. Veal,[2] F. Fuchs,[3] V. Muñoz-Sanjosé,[4] F. Bechstedt,[3] C. F. McConville,[2] and Kevin E. Smith[1,†]

[1]*Department of Physics, Boston University, 590 Commonwealth Avenue, Boston, Massachusetts 02215, USA*
[2]*Department of Physics, University of Warwick, Coventry CV4 7AL, United Kingdom*
[3]*Institut für Festkörpertheorie und -optik, Friedrich-Schiller-Universität, Max-Wien-Platz 1, 07743 Jena, Germany*
[4]*Departamento de Fisica Aplicada y Electromagnetismo, Universitat de Valéncia, C/Dr. Moliner 50, 46100 Burjassot, Spain*
[5]*Advanced Light Source, Lawrence Berkeley National Laboratory, Berkeley, California 94720, USA*

The electronic structure of well-ordered single-crystal thin films of CdO(100) has been studied using angle-resolved photoemission spectroscopy. Quantized electron subbands are observed above the valence-band maximum. The existence of these states provides evidence of an intrinsic electron accumulation space-charge layer near the CdO surface, an interpretation supported by coupled Poisson-Schrödinger calculations. The origin of the accumulation layer result is discussed in terms of the bulk band structure of CdO calculated using quasiparticle-corrected density-functional theory, which reveals that the conduction-band minimum at the Brillouin-zone center lies below the charge neutrality level.

PACS number(s): 79.60.Bm

I. INTRODUCTION

There is great interest in the current and potential uses of metal oxides in electronic devices. This is motivated by the electronic, magnetic, and optical phenomena displayed by metal oxides that are absent from conventional inorganic semiconductors. A fundamental understanding of the relevant metal oxide electronic structure is thus crucial. A specific class of metal oxides that has already seen widespread application is transparent conducting oxides (TCOs).[1] These combine electrical conductivity and optical transparency and are essential for photovoltaic and optoelectronic applications. However, the standard TCO in commercial use, indium tin oxide, has many undesirable properties, and there is a drive to develop new TCOs.[1] In this regard, post-transition-metal oxides with wide optical gaps and the ability to sustain high concentrations of electrons with high mobility are being explored. Among the post-transition-metal oxides, CdO and CdO-derived alloys have received much attention.[2] However, the interfacial electronic structure of CdO and derived alloys is not well understood.

We report here an experimental study of the surface electronic structure of well-ordered single-crystal thin-film rocksalt-phase *n*-type CdO(100). Specifically, we report the observation of an electron accumulation layer near the surface of CdO. Furthermore, not only are there excess electrons (over the bulk density) near the CdO(100) surface, we have discovered that these electrons reside in quantum well states, trapped in an intrinsic one-dimensional potential perpendicular to the surface. The presence of quantized electron accumulation subband states near the surface of *n*-type CdO(100) has significant implications for contact formation and device use of CdO-derived materials.

The quantized subbands were directly observed using angle-resolved photoemission spectroscopy (ARPES).[3] The existence of these subbands, above the valence-band maximum (VBM), reveals intrinsic electron accumulation at *n*-type CdO surfaces. We explain the electron accumulation in terms of the bulk electronic structure of CdO, calculated using quasiparticle-corrected density-functional theory (DFT). ARPES studies recently revealed quantized electron subbands within the electron accumulation layer formed at InN surfaces.[4] The origin of electron accumulation in inorganic semiconductors is a very low conduction-band minimum (CBM) compared to the rest of the conduction-band edges across the Brillouin zone, lying below the charge neutrality level.[5] Our calculations show a similarly low CBM in CdO. These results suggest the possibility of intrinsic electron accumulation at the surfaces of other TCOs such as In_2O_3, SnO_2, and ZnO, which are also expected to have low CBMs.

II. EXPERIMENTAL DETAILS

The experiments were undertaken on undulator beamline 12.0.1 at the Advanced Light Source (ALS), Lawrence Berkeley National Laboratory. This beamline is equipped with a 100 mm hemispherical electron energy analyzer (Scienta SES100). Typical electron energy and full angular resolution were 35 meV and 0.5°, respectively. Single-crystalline CdO(100) films were grown on *r*-plane sapphire by metal-organic vapor phase epitaxy. The films were 380 nm thick and had a surface area of 5 mm^2. Details of the growth and characterization of the samples are reported elsewhere.[6] Infrared reflectivity, optical absorption, and single-field Hall-effect measurements from these samples indicate a room-temperature band gap of 2.16 ± 0.02 eV and a band-edge effective mass of $0.21 \pm 0.01m_0$.[7] Prior to insertion into the ultrahigh vacuum (UHV) spectrometer system (base pressure $<1 \times 10^{-10}$ torr), the samples were treated by an ultrasonic rinse of acetone and isopropanol. Samples were then annealed for 2 h at 600 °C in UHV. All surfaces exhibited sharp (1×1) low-energy electron-diffraction (LEED) patterns with a low background. Core level photoemission spectra could not be recorded due to the photon energy range
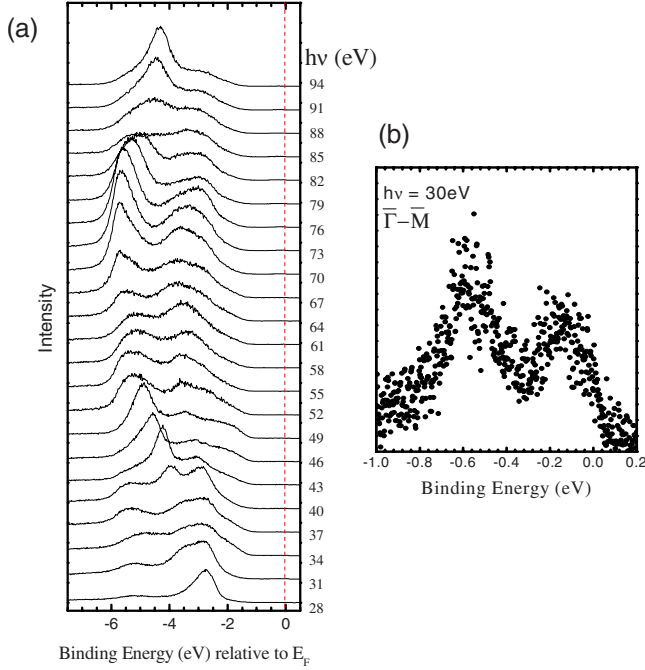
FIG. 1. (Color online) (a) Normal-emission ARPES EDCs, probing states along the Γ-X direction of the bulk Brillouin zone (illustrated in Fig. 2) for a range of incident photon energies $h\nu$ from 28 to 94 eV. (b) EDCs recorded for states within 1 eV of E_F with an incident photon energy $h\nu$=30 eV. The vertical scale is magnified 50 times from that used in (a).
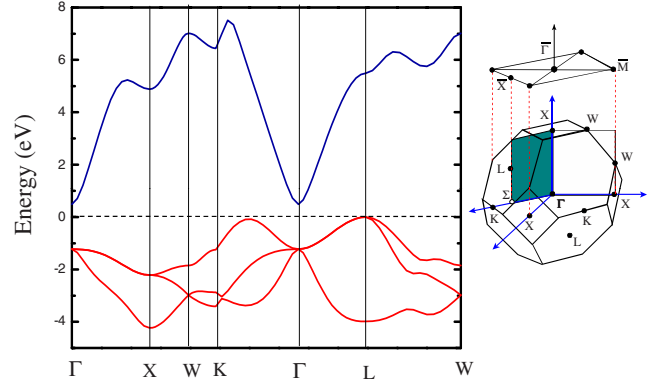
FIG. 2. (Color online) Quasiparticle-corrected DFT calculated bulk band structure of CdO, displaying its extremely low Γ-point CBM. The bulk and surface Brillouin zones are also illustrated.

available on beamline 12.0.1. The ARPES data presented here were recorded at room temperature and are referenced relative to the Fermi level (E_F) of an atomically clean gold foil in contact with the sample. Hall-effect measurements made following the ARPES experiments indicated a carrier density and mobility of $n \sim 3 \times 10^{19}$ cm^{-3} and $\mu \sim 90$ cm^2 V^{-1} s^{-1}.

III. THEORETICAL DETAILS

Band-structure calculations were performed within the framework of hybrid DFT using the recently proposed HSE03 functional for exchange and correlation.[8] Quasiparticle effects were taken into account by a subsequent GW correction of the HSE03 eigenvalues using many-body perturbation theory. In the GW calculations, the Coulomb potential was fully screened using the random-phase approximation (RPA) dielectric function based on the HSE03 eigenvalues and functions.[9] It has been shown that this combination of DFT+HSE03 and GW calculations provides excellent values for the fundamental gaps and semicore d levels of many semiconductors.[10] Furthermore, the calculated O $2p$ partial density of states and the energetic location of the hybridized Cd $4d$-O $2p$ level agrees well with recent O K-edge x-ray emission spectra of single-crystalline thin-film CdO.[11]

IV. RESULTS

Figure 1(a) presents a series of normal-emission ARPES energy distribution curves (EDCs) for a range of incident

photon energies from $h\nu$=28 eV to $h\nu$=94 eV. A number of dispersive band features are visible, as well as nondispersive density of state features. Figure 2 presents the quasiparticle-corrected bulk band-structure calculations for CdO, with the bulk and surface Brillouin zones shown in the inset. These calculations indicate that there is one triply-degenerate band at the valence-band maximum at the Brillouin-zone center Γ that splits into one doubly-degenerate band and one singly-degenerate band that disperse to higher binding energies as k is varied along Γ-X.[11,12] This is the direction in the bulk Brillouin zone that is probed in a normal-emission ARPES measurement from the (100) surface as the incident photon energy is varied. The EDCs in Fig. 1(a) clearly show one feature at the top of the valence-band emission at about 2.75 eV below E_F for the spectrum recorded with $h\nu$=28 eV. This splits into two features that move to higher binding energy as the photon energy is increased, reaching a maximum binding energy when the photon energy is at 67 eV. As the photon energy is increased further, these two features disperse back to lower binding energy, reforming one degenerate peak at $h\nu$=85 eV. From this behavior, we associate the features in the EDCs recorded at 28 and 85 eV as due to the electronic structure at the bulk Γ points in adjacent Brillouin zones. Remarkably, the normal-emission spectra for photon energies near these values exhibit two clear, though weak, spectral features *above* the valence-band maximum, close to E_F. This is shown in Fig. 1(b), which presents an EDC recorded with $h\nu$=30 eV; only the photocurrent from states within 1 eV of E_F is presented and the vertical intensity scale is magnified in Fig. 1(b) by a factor of 50 compared to Fig. 1(a). [Note that other spectral features are visible in Fig. 1(a) aside from emission from the two bulk bands. These may be density of states features, surface defects, or due to residual impurities on the CdO surface.[3] A study of the origin of these features is planned. Their presence does not impact the states above the CBM.]

To further probe the nature of the states near the Fermi level, high-resolution ARPES spectra were recorded at $h\nu$=30 eV and the momentum of the states parallel to the surface ($k_{\parallel}$) were measured. Figure 3(a) presents photocurrent intensity maps from states with a binding energy within 1.1 eV of E_F and with $k_{\parallel}$ varied along the $\bar{\Gamma}$-$\bar{M}$ direction in the
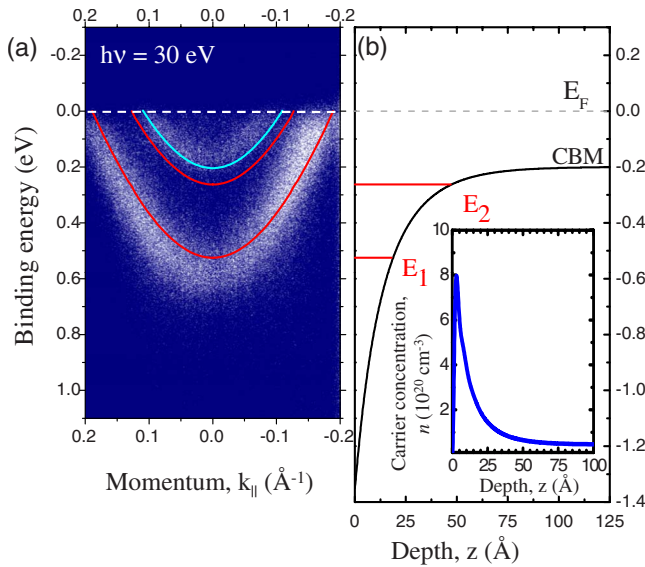
FIG. 3. (Color online) (a) ARPES photocurrent intensity map of the near-Fermi-level emission for $h\nu = 30$ eV, recorded at room temperature. (b) The coupled Poisson-Schrödinger calculated downward band bending near the surface of CdO. For comparison, the calculated subband (E_1 and E_2) and bulk conduction-band (topmost) dispersions are plotted within (a). The carrier-concentration variation near to the surface caused by the downward band bending is shown in the inset of (b). Note that the carrier density reaches zero at the surface.

surface Brillouin zone, recorded with $h\nu = 30$ eV. The photocurrent intensity map for states along the $\bar{\Gamma}$-$\bar{X}$ direction was also measured and displayed similar dispersion. Two distinct bands with positive nonparabolic dispersions are observed in the photocurrent intensity map in Fig. 3(a). Strikingly similar spectral features above the VBM have previously been observed with ARPES from the narrow gap semiconductor InN and were associated with quantized electron subbands within an intrinsic electron accumulation layer.[4] Fermi-level pinning results in the conduction and valence edges bending to achieve overall charge neutrality.[13] The downward band bending associated with this electron accumulation creates a confining potential normal to the surface. This, coupled with the effectively almost infinite potential barrier of the surface, causes the conduction-band states to become quantized in the direction normal to the surface, forming two-dimensional subbands. Such subbands observed in Figs. 1 and 3 indicate that the electrons are quantized within an electron accumulation layer formed at the surface of CdO.

V. DISCUSSION

In order to model the states in the accumulation layer, we performed nonparabolic coupled Poisson-Schrödinger calculations of quantized electron accumulation layers at the CdO surface. The band bending potential is determined by solving Poisson's equation within a modified Thomas-Fermi approximation, subject to the boundary conditions of the total band bending at the surface and the bulk Fermi level. The Schrödinger equation is then solved for the resulting one-

electron potential to yield subband energies and dispersion relations. The inclusion of conduction-band nonparabolicity has recently been shown to be important for CdO,[7] especially in this case due to the high carrier concentrations present in an accumulation layer. This has been included here via the Kane $\mathbf{k} \cdot \mathbf{p}$ approximation.[14] Further details of the coupled Poisson-Schrödinger calculations are reported elsewhere.[15] The CdO material parameters used here are from Ref. 7. The best agreement between the observed subbands in the ARPES photocurrent maps and the calculated subband energies and dispersions was achieved for a bulk carrier concentration of 4.5×10^{19} cm^{-3} and a downward band bending of 1.15 eV, corresponding to a density of 9×10^{13} cm^{-2} positively charged surface states.

The conduction-band edge and carrier-concentration variation (as a function of depth) resulting from these simulations are shown alongside the data in Fig. 3(b). A large increase in carrier concentration (i.e., an electron accumulation) to $\sim 8 \times 10^{20}$ cm^{-3} is evident in the near-surface region, as shown within the inset of Fig. 3(b). Note that the carrier concentration still tends to zero right at the surface as this acts as an effectively infinite potential barrier. The resultant Schrödinger equation solutions for the one-electron band bending potential yield subbands located 0.53 and 0.26 eV below E_F (at $\mathbf{k}_{\parallel} = 0$ Å^{-1}), close to the subband minima in the experimental spectra. Additionally, the dispersion of the calculated subbands agrees well with the experimental spectra as shown in Fig. 3(a), in particular, the increasing linearity of the dispersion as $\mathbf{k}_{\parallel}$ moves further away from Γ due to the $\mathbf{k} \cdot \mathbf{p}$ interaction between the conduction and valence bands. The calculated subband-edge effective masses are approximately $0.23 m_0$ and $0.22 m_0$ for the lower (E_1) and upper (E_2) subbands, respectively. It should be noted that the upper subband E_2 is only weakly bound, being located close in energy to the bulk conduction-band edge. Thus, it cannot be clearly resolved in the experimental spectra from the bulk conduction-band dispersion plotted in Fig. 2(b). The small differences between the calculated subbands and the measured spectra are attributed to approximations involved within the calculations. In particular, for the very high carrier concentrations associated with the peak density of the accumulation layer, the $\mathbf{k} \cdot \mathbf{p}$ approximation may deviate from the true conduction-band dispersion. Additionally, an increase in many-body effects such as electron-electron and electron-impurity interactions, leading to band-gap renormalization, may also cause deviations between the experiment and model, again due to the high carrier concentrations in the accumulation layer. Finally, variations in bulk carrier density can also cause changes in the subbands.

The sheet density associated with the electrons in the quantized subband states can also be directly estimated from the measured Fermi wave vectors $\mathbf{k}_F$ of the subbands. Under the assumption of strict two dimensionality, the area of a circular two-dimensional Fermi surface is related to the number density of electrons in the accumulation layer by the relation

$$n_{2D} = \frac{k_F^2}{2\pi}. \tag{1}$$

From the data presented in Fig. 3, and constant energy photocurrent contours (not shown), the $\mathbf{k}_F$ for the subbands are

measured to be 0.2 and 0.1 Å^{-1} for the first and second bands, corresponding to an electron sheet density of 6.4×10^{13} cm^{-2} and 1.6×10^{13} cm^{-2}, respectively, giving a combined areal density of approximately 8×10^{13} cm^{-2} due to the subband states. This is in agreement with the surface-state density obtained from the coupled Poisson-Schrödinger calculations, supporting the assignment of the subbands as due to an electron accumulation layer at the CdO surface.

The mechanism driving the accumulation of electrons at the surface of CdO can be understood from its calculated bulk band structure (shown in Fig. 2). The breaking of the bulk translational symmetry at the surface allows evanescent surface states to exist within the semiconductor band gap, whose wave functions decay exponentially into the vacuum.[13] Although the exact distribution of these virtual gap states (ViGSs) is specific to a given surface reconstruction and the presence of any adatoms on the surface, some general remarks can be made. The ViGSs derive from the bulk band structure and so they are predominantly donorlike close to the valence band and acceptorlike close to the conduction band. As the ViGSs are localized at the surface, their character is determined from contributions from across the entire Brillouin zone and not just the valence and conduction-band extrema. This is in contrast to the bulk electrical properties of semiconductors, which tend to be dominated by relatively few electrons close to the CBM or holes close to the VBM. The charge neutrality level (CNL) marks the energy at which the character of the ViGS changes from predominantly donorlike (below) to acceptorlike (above). Due to the localized real-space, and hence extended k-space, nature of the ViGS, the CNL therefore lies close to the average midgap energy across the Brillouin zone.[16]

Quasiparticle-corrected bulk band-structure calculations for CdO (Fig. 2) reveal that the CBM at the Γ point is extremely low compared to the average conduction-band edge across the entire Brillouin zone. From the preceding argument, the CNL should lie significantly above the CBM in CdO, above the energy of typical bulk Fermi levels.[7] E_F will therefore pin close to, but slightly below, the CNL at the surface of CdO. Consequently, a number of donor ViGSs will be unoccupied at the surface leading to a positive surface charge. The unoccupied ViGS will be resonant with bulk conduction-band states allowing the ViGS to donate their electrons directly into the conduction band, leading to a large accumulation of electrons at the surface. Charge neutrality is maintained by a downward bending of the bands at the surface (the negative space-charge of the accumulation layer balances the positive surface charge). Due to the extreme downward band bending present, the conduction-band states in the accumulation layer are quantized into subbands, as observed in the ARPES measurements discussed above.

We consider the situation here to reflect *intrinsic* electron accumulation at CdO, in the same manner as that for InAs (Ref. 17) and InN.[5] Near-surface electron accumulation occurs naturally for these compounds for typical doping limits (i.e., $n < \times 10^{20}$ cm^{-3}) and without additional surface preparation other than *in situ* annealing. Naturally, the space-charge layer of CdO could be further manipulated by varying the bulk doping limits and/or thin layer alkali-metal deposition. For InAs(100), we also note that the surface-state density may differ between surface reconstructions [e.g., the As-rich (2×4) is greater than for the In-rich (2×4) reconstruction],[18] but electron accumulation is present for both cases within the above criterion. In the same manner, surface reconstruction and preparation may play a role in the final surface sheet density, but the separation between the CNL and bulk Fermi level is considered a more significant factor. Therefore, we refer to this case as intrinsic due to the location of the CNL above the CBM of CdO [as for InAs (Ref. 17) and InN (Ref. 5)].

VI. CONCLUSION

Angle-resolved photoemission spectroscopy has been used to image quantized conduction-band subband states at the (100) surface of clean single-crystalline CdO. These states are evidence of an extreme surface electron accumulation, with a high surface-state density of 9×10^{13} cm^{-2} estimated from model calculations of the quantized accumulation layer. The model calculations reveal good agreement with the experimental subband energies and dispersions. The overriding mechanism driving the accumulation of electrons at the surface of CdO was identified as the particularly low Γ-point conduction-band minimum, revealed from quasiparticle-corrected density-functional theory band-structure calculations, causing the conduction-band minimum to lie below the charge neutrality level. This result has major implications for TCO-based technologies.

*Also at Centre de Recherche sur l'Hétéro-Epitaxie et ses Applications (CRHEA), Centre National de la Recherche Scientifique (CNRS), Rue Bernard Gregory, 06560 Valbonne, France.

†ksmith@bu.edu

[1] T. Minami, Semicond. Sci. Technol. **20**, S35 (2005).

[2] Y. Yang, S. Jin, J. E. Medvedeva, J. R. Ireland, A. W. Metz, J. Ni, M. C. Hersam, A. J. Freeman, and T. J. Marks, J. Am. Chem. Soc. **127**, 8796 (2005).

[3] *Angle Resolved Photoemission*, edited by S. D. Kevan (Elsevier, Amsterdam, 1991); K. E. Smith and S. D. Kevan, Prog. Solid State Chem. **21**, 49 (1991).

[4] L. Colakerol, T. D. Veal, H. K. Jeong, L. Plucinski, A. DeMasi, T. Learmonth, P. A. Glans, S. Wang, Y. Zhang, L. F. J. Piper, P. H. Jefferson, A. Fedorov, T. C. Chen, T. D. Moustakas, C. F. McConville, and K. E. Smith, Phys. Rev. Lett. **97**, 237601 (2006).

[5] I. Mahboob, T. D. Veal, L. F. J. Piper, C. F. McConville, H. Lu, W. J. Schaff, J. Furthmuller, and F. Bechstedt, Phys. Rev. B **69**, 201307(R) (2004); I. Mahboob, T. D. Veal, C. F. McConville, H. Lu, and W. J. Schaff, Phys. Rev. Lett. **92**, 036804 (2004).

[6] J. Zuniga-Perez, C. Munuera, C. Ocal, and V. Munoz-Sanjose, J. Cryst. Growth **271**, 223 (2004).

[7] P. H. Jefferson, S. A. Hatfield, T. D. Veal, P. D. C. King, C. F. McConville, J. Zúñiga-Pérez, and V. Munoz-Sanjose, Appl. Phys. Lett. **92**, 022101 (2008).

[8] J. Heyd, G. E. Scuseria, and M. Ernzerhof, J. Chem. Phys. **118**, 8207 (2003).

[9] M. Shishkin and G. Kresse, Phys. Rev. B **74**, 035101 (2006).

[10] F. Fuchs, J. Furthmuller, F. Bechstedt, M. Shishkin, and G. Kresse, Phys. Rev. B **76**, 115109 (2007).

[11] L. F. J. Piper, A. DeMasi, K. E. Smith, A. Schleife, F. Fuchs, F. Bechstedt, J. Zuniga-Perez, and V. Munoz-Sanjose, Phys. Rev. B **77**, 125204 (2008).

[12] A. Schleife, F. Fuchs, J. Furthmuller, and F. Bechstedt, Phys. Rev. B **73**, 245212 (2006).

[13] W. Monch, *Semiconductor Surfaces and Interfaces* (Springer, Berlin, 2001).

[14] E. O. Kane, J. Phys. Chem. Solids **1**, 249 (1957).

[15] P. D. C. King, T. D. Veal, and C. F. McConville, Phys. Rev. B **77**, 125305 (2008).

[16] J. Tersoff, Phys. Rev. Lett. **52**, 465 (1984).

[17] L. F. J. Piper, T. D. Veal, M. J. Lowe, and C. F. McConville, Phys. Rev. B **73**, 195321 (2006).

[18] M. Noguchi, K. Hirakawa, and T. Ikoma, Phys. Rev. Lett. **66**, 2243 (1991).